FACTA UNIVERSITATIS
Series: **Electronics and Energetics** Vol. 39, Nº 1, March 2026, pp. 1 - 12
https://doi.org/10.2298/FUEE2601001K

Invited Paper

MICROWAVE SENSOR ARRAY BASED ON SPLIT RING RESONATORS FOR TUMOR DETECTION AND LOCALIZATION

Anja Kovačević, Nikola Basta, Milka Potrebić Ivaniš

University of Belgrade – School of Electrical Engineering, Belgrade, Serbia

ORCID iDs: Anja Kovačević https://orcid.org/0000-0002-6648-8331
Nikola Basta https://orcid.org/0000-0001-6141-7414
Milka Potrebić Ivaniš https://orcid.org/0000-0002-4866-6608

Abstract. *A microwave sensor array for tumor detection and localization was designed and fabricated on an FR-4 substrate. The sensor consists of three square-shaped split-ring resonators coupled to a microstrip feeding line. Each sensing cell produces a stopband in the transmission spectrum of the device. The sensing cells are mutually decoupled, so that the deposition of the sample on one of the cells induces shift of resonant frequency of only that cell, thereby enabling spatial resolution. The sensing performance was experimentally verified with the samples of animal tissues in an ex vivo setting. Pork fat and lean tissues were used for preparing the samples, since the dielectric contrast between them roughly corresponds to the contrast between healthy and tumorous tissue. Experimental results suggest that the designed sensor can be effectively used for tumor detection and localization.*

Key words: *Biosensors, Tissues, Tumors, Split-ring resonators, Tumor detection, Tumor localization*

1. INTRODUCTION

Alongside traditional applications such as wireless communication, satellite and radar systems, microwave technology has also been successfully employed in material sensing and particularly in biomedicine and healthcare settings for both diagnostic and therapeutic purposes [1]−[2]. In biomedical applications, propagation media for microwaves are biological materials that are distinctly inhomogeneous and susceptible to anatomical, physiological and biochemical variations [2]. Consequently, the main challenge in using microwaves for such applications is understanding the interaction between electromagnetic (EM) waves and biological materials and translating that knowledge into effective system design.

Received November 21, 2025; accepted November 21, 2025
Corresponding author: Milka Potrebić Ivaniš
University of Belgrade – School of Electrical Engineering.
E-mail: milka.p@mts.rs

Interactions between EM waves and biological materials can be of thermal or non-thermal character. Applications based on thermal interactions include sterilization of laboratory and medical equipment, microwave ablation therapy used to treat malignant tumors in the liver, kidney, lung and bone tissues [3], and controlled heating treatments against viruses such as human papilloma virus [4]. Microwave therapies can increase the effectiveness of treatment, reduce the discomfort and shorten recovery time [2]. Non-thermal interactions are of great significance in medical diagnostics where antennas and microwave sensors are used for microwave imaging, biosensing, diagnosis of malignant tumors and real-time analysis of body fluids [2],[4].

Non-invasive characterization of biological materials and living systems can be performed by sensors that exploit the non-thermal wave-matter interaction. These sensors can be designed to operate in different parts of the EM spectrum. The choice of operating frequency depends on the specific sensing application, where a compromise must be made between the achievable resolution, the penetration depth into the material under test (MUT), the device size, and the cost of its manufacture. Shorter waves, such as ultraviolet, cause damage to DNA and proteins due to their ionizing nature, which makes them unsuitable for biomedical applications [4]. On the other hand, longer waves, such as microwave and terahertz (THz) waves, are classed as non-ionizing and are much safer for biological MUTs. Although THz sensors offer high resolution and are relatively small in size [5]−[8], they suffer from low penetration depth into the MUT due to strong EM absorption at high frequencies and relatively high manufacturing costs. In contrast, microwave sensors are less expensive to manufacture and operate at even longer wavelengths, which can penetrate more deeply into the MUT.

Various designs of microwave sensors for biosensing have already been investigated. A planar sensor with a printed spiral presented in [9] was designed to determine the concentration of D-glucose in pig blood. Microwave sensors based on coplanar waveguides [10], and electric-LC resonators [11] were tested for real-time glucose detection. Differential sensors constitute a distinct class of sensors whose sensing principle relies on symmetry between two sensing elements [12]. Microwave sensors with split-ring resonators (SRR) of various shapes were designed for organic tissue analysis and ablation therapy [13]−[14].

The organic tissue analysis for tumor detection and localization utilizing microwave sensors represents a promising cost-effective addition to the traditional methods for diagnostics such as computerized tomography (CT), X-rays and magnetic resonance imaging (MRI) [15]. Detection of a tumor in the surrounding healthy tissue is based on the dielectric contrast between them. The relative permittivity of abnormal tissue is approximately 10 – 30% higher compared to healthy tissue [14]. On the other hand, localization of abnormality benefits from the sensor's ability to perform spatial mapping of tissue under test (TUT), which can be taken into consideration during the design process. The ability of spatial mapping is achieved by integrating individual sensing elements into an array. In [16], a 10×10 electronically controlled complementary spiral-resonator array for skin tumor detection was investigated. The experimental results demonstrated that the array can detect tumor tissue as small as 10 mm in diameter. A multi-layer metasurface loop-dipole sensor array for near-field breast tumor detection was considered in [17], showing that it can detect tumorous tissues in breast phantoms placed closely to the sensor. The frequency-multiplexed planar sensor arrays, described in [15], [18], [19], are simpler and more cost-effective, but still proven to be efficient solutions to extract the position of the abnormality.

In our previous works, we have designed a two-cell planar touch sensor for wearable applications [18] and a six-cell microwave sensor for tissue differentiation [19]. With the sensor from [19], we were able to detect the positions and distinguish two types of deposited cube-shaped animal tissue samples (muscle or fat) using a low-cost network analyzer.

In this study, a planar frequency-multiplexed microwave sensor array of three SRR-based sensing cells is fabricated, and its sensing performance is evaluated using a slab of animal fat tissue, into which small muscle tissue abnormalities are introduced. The sensor design, alongside its principle of operation, is discussed in Section 2. A fabricated prototype and experimental results are presented in Section 3. The most important results of this work are summarized in Section 4, along with further research directions.

2. SENSOR DESIGN

The microwave sensor proposed in this study is a planar structure designed for direct contact with TUT in either *ex vivo* or *in vivo* scenarios. It consists of three sensing cells that are coupled to a microstrip feeding line (Fig. 1). The sensing cells are square-shaped SRRs with three gaps. Dimensions of the sensor presented in Fig. 1 are given in Table 1. The sensor is printed on the FR-4 substrate with the following parameters: $\varepsilon_r = 4.5$, $\tan\delta = 0.019$, thickness $h = 1.5$ mm and metallization thickness $t = 0.035$ mm.

The sensing principle is based on the strong response of SRR to the incident EM field and can be considered from two different, but mutually correlated perspectives. The circuit-based perspective implies modeling of SRR as an LC resonant cell (if losses are neglected) coupled to a microstrip feeding line. Inductivity of SRR comes from the conductive square-shaped ring. The SRR's capacitance mainly stems from the gaps, which act as plate capacitors in the first approximation. Depositing the TUT sample on the gap increases the effective permittivity of the dielectric in the gap and therefore its capacitance. Consequently, the resonant frequency of SRR is shifted towards the lower frequencies. Samples with different electrical properties induce different resonant frequency shifts, thus leaving a unique footprint in the response.

From the antenna-based perspective, the SRR can be regarded as a half-wavelength dipole antenna with L-shaped capacitive loads on both sides. The antenna is excited by a signal propagating through a coupled microstrip line. The capacitive loads provide non-zero currents at the ends of a dipole, ensuring the strong interaction with the TUT sample in the lateral gaps, which represent the sensitive regions of the sensing cell. The bottom gap is not affected by the sample, as the wave-sample interaction there is fairly limited due to the weak EM field. The antenna-based perspective helps identify the sensor's sensitive regions, which is fairly difficult to determine from a circuit-based perspective.

During the design process, the sensor was modeled in circuit simulator AWR Microwave Office and in software for 3D EM analysis WIPL-D Pro [20], [21]. A comparison between the transmission spectrums obtained from AWR Microwave Office and WIPL-D Pro is shown in Fig. 2. From this figure, it can be concluded that the circuit simulator gives sufficiently accurate results and can therefore be used for sensor design, which is in accordance with previously reported results [15].

Each sensing cell produces its own stopband in the transmission spectrum, centered around its resonant frequency. The width of a stopband is determined by the strength of

coupling between the feeding line and the corresponding SRR. To achieve narrow stopbands, which are highly desirable for sensing applications, the width of the gap between the feeding microstrip line and SRR should be carefully chosen. If that gap is too wide, the SRR will be completely isolated from the line (the equivalent dipole antenna will remain without excitation). On the contrary, if the feeding line and SRR are too close, the coupling will be excessively strong, which will result in a wide stopband [22].

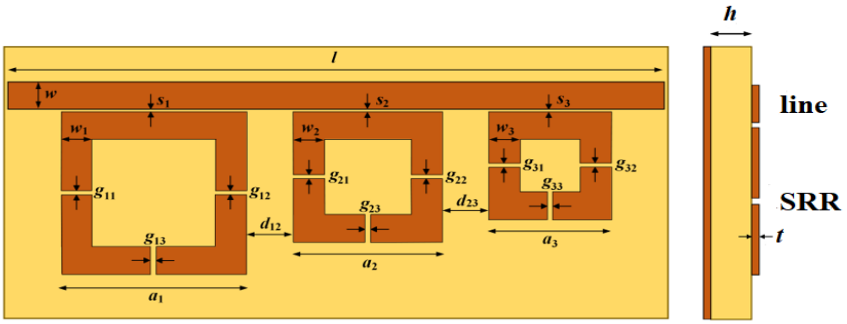

Fig. 1 The proposed microwave sensor – view from above (on the left) and cross section (on the right)

Table 1 Sensor dimensions (in mm)

a_1	17.1
a_2	13.7
a_3	11.3
$g_{11}, g_{12}, g_{13}, g_{21}, g_{22}, g_{23}, g_{31}, g_{32}, g_{33}$	0.5
s_1, s_2, s_3	0.3
w, w_1, w_2, w_3	2.8
d_{12}, d_{23}	4.5
l	61.1

To obtain spatial resolution, the sensing cells must be mutually decoupled so that the response of one cell does not affect the response of the others. The independence of sensing cells is ensured during the design process by choosing an appropriate distance between neighboring SRRs ($d = 3h, d \in \{d_{12}, d_{23}\}$). As a result of decoupling, the presence of a sample on one sensing cell alters only the peak that corresponds to that cell, while other peaks remain unchanged. Therefore, a spatially resolved reconstruction of the sample can be performed. The number of pixels in the reconstruction is equal to the number of sensing cells. Additionally, each resonance can be tuned independently, which can significantly shorten the analysis time, especially when using a full-wave simulator.

During the design process, it is necessary to choose the operating frequency range. The upper frequency limit f_u (for the proposed sensor f_u = 5.2 GHz) determines the number of sensing cells. If a sensing cell resonates at frequency f, it also resonates at frequencies kf, where k is a positive integer. Consequently, to ensure the independence of resonances and unambiguous sample localization, the first resonant frequency f_1 must be greater than $f_u/2$. Additionally, resonances cannot be too close to each other, since the presence of the sample

induces a frequency shift toward lower frequencies. That frequency shift is determined by the electrical properties of the TUT sample. For example, if a sample deposited on the second sensing cell induces a frequency shift larger than $f_2 - f_1$, the second peak will move ahead of the first one, and it will be incorrectly concluded that the sample is located on the first sensing cell. The resonances from Fig. 2 are 3.060 GHz, 4.020 GHz and 5.120 GHz for AWR and 3.047 GHz, 4.022 GHz and 5.198 GHz for WIPL-D.

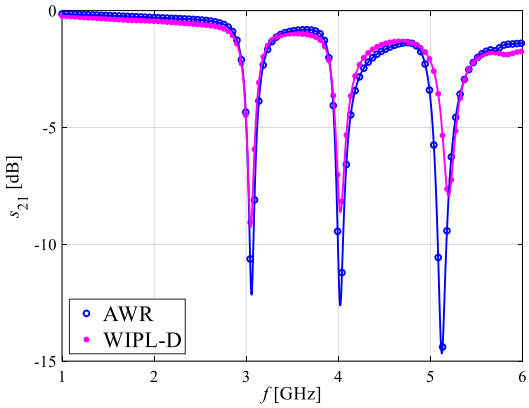

Fig. 2 Comparison of s_{21}-parameters obtained from AWR Microwave Office and WIPL-D Pro

3. Sensor Prototype and Experiment Setup

The sensor prototype was printed on an FR-4 substrate, according to the layout of the design from Fig. 1, created in Altium Designer [23]. The fabricated prototype is presented in Fig. 3. For the preliminary validation, the performance of the fabricated sensor prototype was experimentally tested with animal tissue samples in an *ex vivo* setting.

Pork fat and lean tissue samples that were used for experimental verification are shown in Fig. 4. The contrast between fat and muscle animal tissue roughly corresponds to the contrast between healthy and malignant breast tissue [24]. In *ex vivo* conditions, the contrast between tissues is slightly lower than in *in vivo* conditions due to the lack of blood supply [24]. To preserve a sufficiently large contrast, samples were kept fresh and stored at temperatures below 5°C to reduce water evaporation and maintain the existing water content in the tissue. To prepare the samples shown in Fig. 4, the slab of pork fat tissue was first cut into blocks matching the dimensions of the sensor prototype. Then, holes were punctured in the blocks of fat tissue. Finally, the pieces of muscle tissue that represent tumors were inserted into the punctured holes. One block of fat tissue remained unpunctured to serve as a reference sample of healthy tissue without tumors.

For the measurement of the scattering parameters, a vector network analyzer, Agilent N5227A PNA, was used. To perform measurements with the TUT, an isolation layer was inserted between the sensor and the sample to protect the sensor from the high conductivity of tissue and to facilitate cleaning between uses. For that purpose, a 0.5 mm-thick plastic plate matching the dimensions of the sensor was prepared to act as an isolation layer. The final measurement setup is shown in Fig. 5.

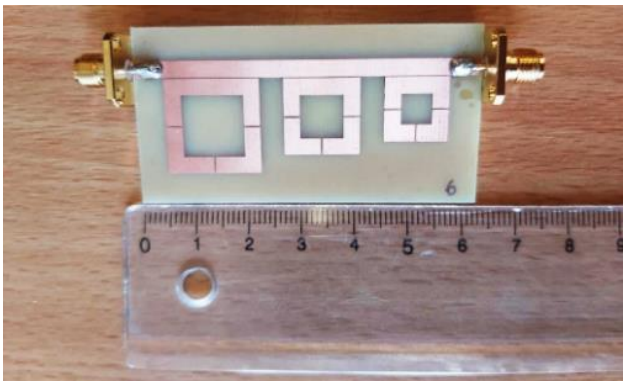

Fig. 3 Fabricated sensor prototype

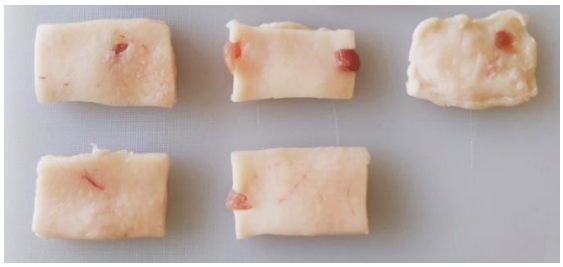

Fig. 4 Samples of animal tissues. Pieces of lean tissue are inserted into the slabs of fat tissue. Bottom left slab is without inserted pieces

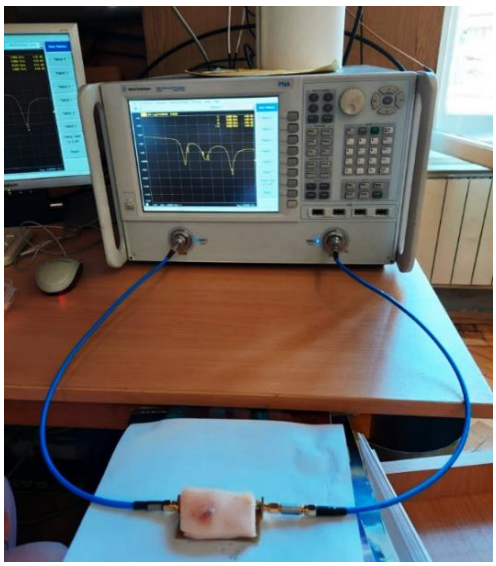

Fig. 5 Setup for s_{21}-parameter measurement. Measurement device is vector network analyzer Agilent N5227A PNA

4. Measurement Results and Discussion

First, the s_{21}-parameter was measured for the sensor without an isolation layer or sample. The comparison between the simulation and measurement results is presented in Fig. 6. The local minima of the prototype's transmission spectrum are slightly shifted in frequency and amplitude compared to the initial design. These differences are due to small deviations in substrate parameters and sensor dimensions.

Then, the reference scenario for tumor detection and localization was simulated. The entire sensor was first covered with a plastic isolation layer and then with a block of fat tissue, which represents healthy tissue without malignancies. The transmission responses measured before and after the addition of the isolation layer and sample are shown in Fig. 7. The obtained results indicate that the isolation layer does not have a significant impact on the response. On the other hand, the addition of a fat tissue layer introduces significant amplitude and frequency shifts in all three stopbands. Resonances of the sensor covered with fat tissue are 2.943 GHz, 3.867 GHz and 4.985 GHz.

Finally, samples with different positions of "tumors" were deposited on top of the isolation layer. Measurement scenarios and results are presented in Figs. 8 – 12. The size of the muscle tissue piece representing the tumor was 4 mm × 4 mm in all scenarios except the one shown in Fig. 13, where a 5 mm × 6 mm muscle tissue piece was placed on the first sensing cell in addition to 4 mm × 4 mm on the third sensing cell. For all measurements, the reference scenario is a sensor covered with an isolation layer and fat tissue.

The results show that the detection and localization of tumors in TUT is possible for all investigated scenarios. If the tumor is placed on the sensitive region of the first sensing cell, as shown in Fig. 8, only the first local minimum, which corresponds to the cell with the tumor, is altered. Similar behavior can be seen in Figs. 9 and 11 for the second and the third sensing cell, respectively. In the scenario from Fig. 10, the tumor affects sensitive regions of the first two sensing cells and introduces changes in both corresponding stopbands. In the scenario shown in Fig. 12, there are two tumors placed on the first and the third sensing cells, which alter the first and the third stopband.

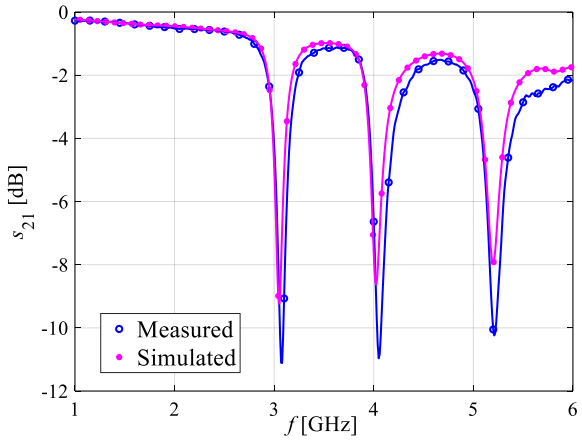

Fig. 6 Comparison between measured and simulated transmission spectrums. Simulated result is from WIPL-D Pro

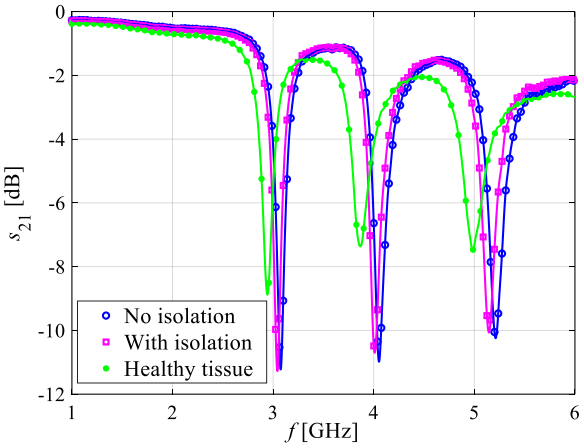

Fig. 7 Transmission spectrums of sensor a) without isolation, b) with isolation and c) with isolation and layer of fat tissue

The lateral gaps of the second and the third sensing cell are the most sensitive to the local changes in TUT due to their higher resonant frequencies. Introducing tumors to those areas causes a decrease in the peak's sharpness and deformities in the peak's shape. Detection and localization of tumor remains possible, but precise reading of the frequency shift becomes more difficult. That can be potentially problematic if the goal is to determine the dielectric properties of TUT using extraction techniques [22].

The measurement results are influenced by several parameters, which can be divided into two basic groups. The first group comprises parameters directly related to the tissue samples, such as freshness and storage conditions. The second group refers to the measurement

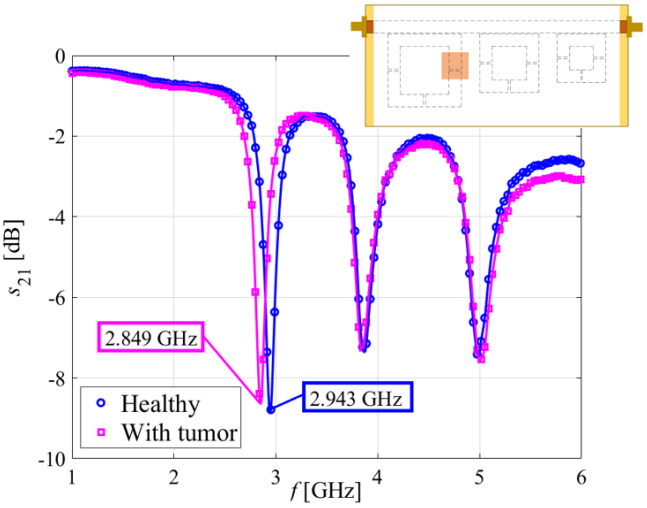

Fig. 8 Measured transmission spectrum of sensor in given scenario with the tumor located on the first sensing cell

procedure itself, as well as the conditions in the room where the measurement is performed. This group includes the positioning of the sample, the contact between the sensor and the isolation, as well as the contact between the isolation and the sample, the room temperature, and the duration of the measurement. Any change in these parameters compared to their state during the experimental verification of the sensor's performance presented in this paper can slightly alter the shown results.

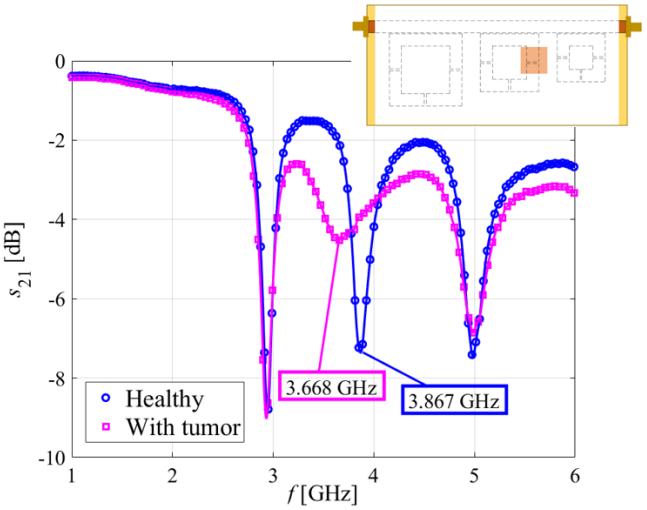

Fig. 9 Measured transmission spectrum of sensor in given scenario with the tumor located on the second sensing cell

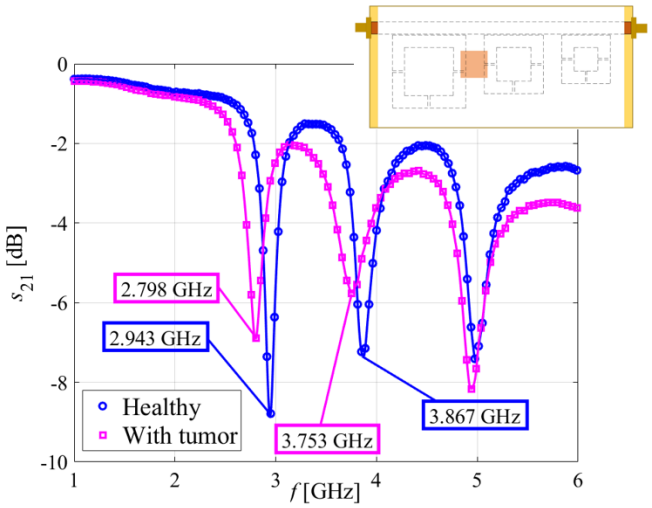

Fig. 10 Measured transmission spectrum of sensor in given scenario with the tumor located in the space between the first and the second sensing cell

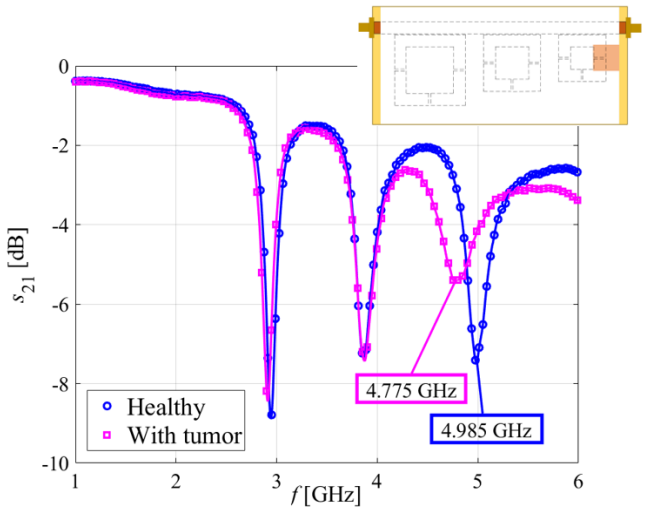

Fig. 11 Measured transmission spectrum of sensor in given scenario with the tumor located on the third sensing cell

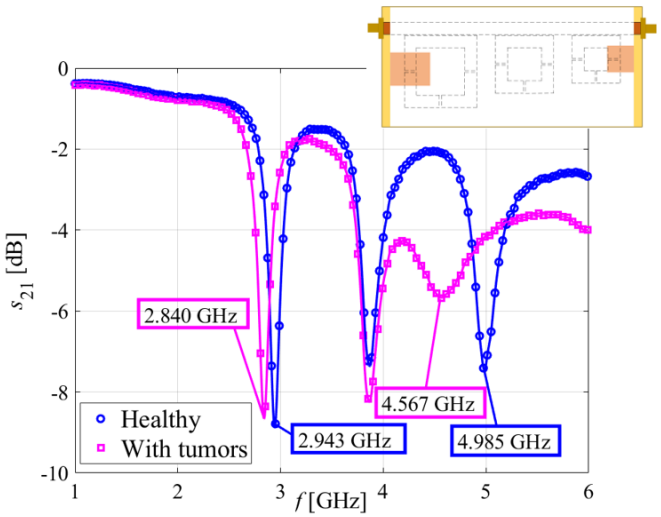

Fig. 12 Measured transmission spectrum of sensor in given scenario with two tumors located on the first and the third sensing cell

5. CONCLUSION

In this paper, a microwave sensor array with three SRR sensing cells coupled to a feeding microstrip line was designed and fabricated for tumor detection and localization. The performance of the fabricated prototype was experimentally verified with samples of animal tissue in an *ex vivo* setting. When the sample is deposited on the sensitive region of the sensor, it changes the resonant frequency of the corresponding sensing cell. The frequency shift depends on the electrical properties of the sample. The tumorous change in the TUT sample is detectable if the dielectric contrast between the tumor and healthy tissue is sufficiently large. The proposed design employs decoupled sensing cells, making their resonant frequencies mutually independent, thus enabling tumor localization. On the example of several animal tissue samples with different positions of simulated tumors, it was shown that the proposed sensor can successfully detect and localize the tumor in the surrounding tissue.

Further research on this sensing technique includes possible design improvements such as miniaturization of the sensor to enable its non-invasive use in *in vivo* conditions, as well as exploiting experimentally obtained data to characterize detected tumorous tissue using an extraction technique.

Acknowledgement: *This work was financially supported by the Ministry of Science, Technological Development and Innovations of the Republic of Serbia under contract number: 451-03-137/2025-03/200103.*

REFERENCES

[1] N. Petrović and P. O. Risman, "Various Diffraction Effects and Their Importance for Detection of Inhomogeneites in Human Tissues," *Facta Universitatis - Series: Electronics and Energetics*, vol. 33, no. 3, pp. 445–458, Sep. 2020.

[2] C. Li, M. Tofighi, D. Schreurs, and T. J. Horng, Principles and Applications of RF/Microwave in Healthcare and Biosensing, Elsevier, 2017.

[3] M. Lubner, C. Brace, J. Hinshaw, and F. Lee Jr, "Microwave Tumor Ablation: Mechanism of Action, Clinical Results and Devices," *J Vasc Interv Radiol*, vol. 21, no. 8, pp. 1–38, Aug. 2010.

[4] A. Gartshore, M. Kidd, and L. T. Joshi, "Applications of Microwave Energy in Medicine", *Biosensors*, vol. 11, no. 4, pp. 1–13, Mar. 2021.

[5] A. Kovačević, M. Potrebić, D. Tošić, "Sensitivity Analysis of Possible THz Virus Detection Using Quad-Band Metamaterial Sensor," In Proceedings of the 2021 IEEE 32nd International Conference on Microelectronics (MIEL), pp. 107–110, Niš, Serbia, Sep, 2021.

[6] A. Kovačević, D. Tošić, M. Potrebić, "Sensitivity Characterization of Multi-Band THz Metamaterial Sensor for Possible Virus Detection," *Electronics*, vol. 11, no. 5, pp. 1–19, Feb, 2022.

[7] A. Kovačević, M. Potrebić, D. Tošić, "The Impact of Finite Dimensions on the Sensing Performance of Terahertz Metamaterial Absorber," *Facta Universitatis - Series: Electronics and Energetics*, vol. 36, no. 1, pp. 17–29, Mar, 2023.

[8] P. Ranjan, N. Mishra, J. Радовановић, M. Potrebić Ivaniš, L. Murmu, J. Kumar Rai, "Refractive index sensing: study and analysis for SARS-CoV-2 detection," *Optical and Quantum Electronics*, vol. 56, no. 7, pp. 1–13, 2024.

[9] H. Melikyan, E. Danielyan, S. Kim, J. Kim, A. Babajanyan, J. Lee, B. Friedman, and K. Lee, "Non-Invasive in vitro Sensing of D-Glucose in Pig Blood," *Medical Engineering & Physics*, vol. 34, no. 3, pp. 299–304, Apr. 2012.

[10] M. C. Cebedio, L. A. Rabioglio, I. E. Gelosi, R. A. Ribas, A. J. Uriz and J. C. Moreira, "Analysis and Design of a Microwave Coplanar Sensor for Non-Invasive Blood Glucose Measurements," *IEEE Sensors Journal*, vol. 20, no. 18, pp. 10572–10581, Sept. 2020.

[11] S. Harnsoongnoen, A. Wanthong, "Coplanar Waveguide Transmission Line Loaded with Electric-LC Resonator for Determination of Glucose Concentration Sensing," *IEEE Sensors Journal*, vol. 17, no. 6, pp. 1635–1640, Mar. 2017.

[12] N. Nikkhah, R. Keshavarz, M. Abolhasan, J. Lipman and N. Shariati, "Highly Sensitive Differential Microwave Sensor Using Enhanced Spiral Resonators for Precision Permittivity Measurement," *IEEE Sensors Journal*, vol. 24, no. 9, pp. 14177–14188, May 2024.

[13] C. G. Juan et al., "Study of Q_u-Based Resonant Microwave Sensors and Design of 3-D-Printed Devices Dedicated to Glucose Monitoring," *IEEE Transactions on Instrumentation and Measurement*, vol. 70, pp. 1–16, 2021, Art no. 8005716, doi: 10.1109/TIM.2021.3122525.

[14] M. Puentes, M. Maasch, M. Schüßler, C. Damm, and R. Jakoby, "Analysis of Resonant Particles in a Coplanar Microwave Sensor Array for Thermal Ablation of Organic Tissue," In Proceedings of the IEEE MTT-S International Microwave Symposium, 2014.

[15] M. Puentes, C. Weiß, M. Schüßler, and R. Jakoby, "Sensor Array Based on Split Ring Resonators for Analysis of Organic Tissues," Proc. of IEEE MTT-S International Microwave Symposium, 2011.

[16] J. Bai, H. Guo and X. Lai, "An Electronically Controlled Resonant Microwave Sensor Array for Skin Tumor Detection," *IEEE Access*, vol. 13, pp. 102445–102461, 2025.

[17] M. A. Aldhaeebi, T. Almoneef, S. Bamatraf, A.O. Aldhaibain, O. Bakhalah, S. Alhdad, S. Bakhalah, M. K. Saleem, "Near-Field Metasurface Sensor for an Early-Stage Breast Cancer Detection," *Sensors International*, vol. 6, 2025.

[18] A. R. Kovačević, A. Z. Golubović, A. N. Ninković, V. S. Kostić and M. M. Ilić, "Design of an RF Touch Sensor for On-Body Applications," In Proceedings of the 2024 IEEE International Symposium on Antennas and Propagation and INC/USNC-URSI Radio Science Meeting (AP-S/INC-USNC-URSI), Florence, Italy, 2024, pp. 1569–1570.

[19] A. Kovačević, N. Basta and S. Savić, "Low-cost Portable Sensing System for Organic Tissue Detection and Differentiation," In Proceedings of the 2023 IEEE MTT-S International Microwave Biomedical Conference (IMBioC), Leuven, Belgium, 2023, pp. 184–186.

[20] Microwave Office 14.0, Cadence Inc., https://www.cadence.com, National Instruments AWR Design Environment, El Segundo, CA, 2025.

[21] WIPL-D Pro 18.0, http://www.wipl-d.com, 3D Electromagnetic Solver, WIPL-D d.o.o., Belgrade, Serbia, 2025.

[22] M. Puentes Vargas, Planar Metamaterial Based Microwave Sensor Arrays for Biomedical Analysis and Treatment, Springer, 2014.

[23] Altium Designer 22.0, https://www.altium.com/, Printed Circuit Board Software, San Diego, CA, 2025.

[24] A. Martellosio, M. Pasian, M. Bozzi, L. Perregrini, A. Mazzanti, F. Svelto, P. E. Summers, G. Renne, and M. Bellomi, "0.5 – 50 GHz Dielectric Characterization of Breast Cancer Tissues," *Electronics Letters*, vol. 51, no. 13, pp. 974–975, Jun. 2015.